Title

Cooling Design and Thermal Analysis for Thermal Shields of a Cryocooler-Cooled Superconducting ECR Ion Source MARS-D Magnet

Journal

IEEE Transactions on Applied Superconductivity, 36(3)

ISSN

1051-8223

Authors

Wang, L
Benitez, JY
Duran, JC
et al.

Publication Date

2026-05-01

DOI

10.1109/tasc.2025.3631018

Cooling Design and Thermal Analysis for Thermal Shields of a Cryocooler-cooled Superconducting ECR Ion Source MARS-D Magnet

L. Wang, *Member, IEEE*, J. Y. Benitez, J. C. Duran, D. Todd, L. Xu, Y. Yang

***Abstract*—A demonstrative NbTi based Mixed Axial and Radial field System (MARS-D) is being developed for a next-Generation Electron Cyclotron Resonance Ion Source (ECRIS) at Lawrence Berkeley National Laboratory (LBL), which employs a novel closed-loop coil design scheme that more efficiently utilizes conductor fields and extend the application of NbTi for high frequency (up to 45 GHz) ECR operation. The NbTi MARS-D magnet consists of a single hexagonally shaped closed-loop coil and a set of auxiliary solenoids. A cryostat for cooling the MARS-D magnet is under design at LBL. The MARS-D magnet working around 4.2 K will be bath-cooled in liquid helium using multiple two-stage cryocoolers. An intermediate temperature thermal radiation shield is adopted to reduce the heat leakage imposed on 4.2 K coil cold mass from room temperature. The thermal shield is conduction-cooled by the first-stage cold heads of four two-stage cryocoolers and the cold head of a single-stage cryocooler shared with nine binary leads. The temperature in the area of the shield that warm ends of HTS leads are mounted on is expected no higher than 60 K, which is limited by maximum allowable working temperature of HTS leads. The paper presents thermal analysis on the thermal radiation shield including heat loads and effects of eddy current induced during quench on its material selection.**

***Index Terms*—ECRIS, MARS-D magnet, thermal shield, eddy current**

I. INTRODUCTION

THE traditional racetrack-and-solenoid ECRIS structures using NbTi have reached their limit in increasing magnetic fields to achieve higher heating frequencies than 28 GHz. A demonstrative NbTi-based Mixed Axial and Radial field System (MARS-D) is being developed for a next-generation ECRIS operating at up to 45 GHz at LBL, which employs a novel closed-loop coil design scheme that more efficiently utilizes conductor fields and extends the application of NbTi for high-frequency ECR operation [1-3]. The MARS-D magnet is expected to produce a minimum-B configuration with a field maximum of 5.8 T axially and 3.2 T radially. The MARS-D coil cold mass working at 4.2 K is zero-boil-off liquid helium bath-cooled using gravity-driven thermos-syphon cooling circuit and housed in a cryocooler-based cryostat [4].

This work was supported by the U.S. Department of Energy, Office of Science, Office of Nuclear Physics under contract number DE-FOA-0002670. (Corresponding author: Li Wang).

L. Wang is with Lawrence Berkeley National Laboratory, Berkeley, CA 94706 USA (e-mail: liwang-lbl@ lbl.gov).

J. Y. Benitez, J. C. Duran, D. Todd, L. Xu, Y. Yang, are with Lawrence Berkeley National Laboratory, Berkeley, CA 94706 USA.

An intermediate temperature thermal radiation shield is essential to minimize radiation heat leakage from room temperature to the 4.2 K coil cold mass. The thermal shield in the magnet system, typically made of materials with good thermal conductivity and low strength, such as oxygen-free high conductivity (OFHC) copper or high-purity aluminum, must withstand the expected eddy current force during a quench. This paper presents the mechanical behavior of the shield under the Lorentz force generated by eddy currents induced during magnet quench and thermal analyses of the thermal shield. The analyses provide guidance for the preliminary design of the thermal shield.

II. COIL COLD MASS, CRYOSTAT AND THERMAL SHIELD

The NbTi MARS magnet consists of a single hexagonally shaped closed-loop coil and a set of auxiliary solenoids consisting of injection coils, one middle coil, one comb coil and extraction coils, as shown in Fig. 1. The closed-loop-coil are electrically divided into three subsections with different currents to keep it operating further away from the NbTi critical current and achieve higher temperature margins for reliable magnet operation [3]. A shell-based "bladder-and-key" structure is adopted to radially pre-stress the coils of the MARS-D magnet [5-6]. The cold iron yoke made of 1010-steel is applied to enhance the magnetic field and acts as a magnetic shield. Table I lists some of design parameters of MARS-D coils. The coil cold mass is ~2310 kg, 800 mm outer diameter and 798 mm long. The stored magnetic energy is 743.3 kJ.

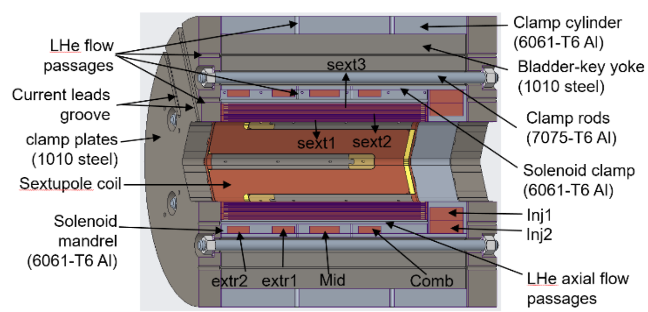

Fig. 1. MARS-D coil cold mass working at 4.2 K.

TABLE I
SOME DESIGN PARAMETERS OF MARS-D COILS

Coil type	Solenoid						Closed-loop coil		
NbTi wire bare / Insulated size	1.36x0.65 mm / 1.45x0.71 mm						1.84x1.16 / 1.91x1.23 mm		
Cu ratio & RRR	1.4, 70						1.3, 90		
Coil name	inj1	inj2	comb	mid	extr1	extr2	sext 1	sext2	sext 3
Layer	38	56	26	26	26	26	8	8	8
Turns per layer	61	61	40	54	40	40	64	64	64
Current density (A/mm^2)	79	227	221	-137	208	208	117	193	193
Jc (4.2K, Bmax) (A/mm^2)	1043	1506	2065	2614	2156	2967	957	1212	1541
Operating current (A)	90	255	255	-156	240	240	310	510	510
Max. field (T)	8.04	7.13	6.06	5.07	5.89	4.48	8.2	7.71	7.06
Tcs (K)	4.97	4.98	5.48	6.17	5.60	6.57	4.8	4.84	5.15

Fig. 2 shows the cross-sectional view of the 3D model of the MARS-D cryostat. Since last summer, significant changes have been made to the cryostat design. Four drop-in-mode integrated PTR450 cryocoolers and one G-M cryocooler AL330 were finally employed due to the uncertain dynamic heat load (potentially up to ~10 W) generated by the plasma beam operating at 45 GHz and the increased design currents of the leads, instead of prior two PT450 cryocoolers. The design currents of nine binary leads were changed from 1x175 A, 3x250 A, 2x300 A, 1x400 A and 2x600 A to 6x300 A and 3x600 A for Cu leads, and from 4x250 A, 3x500 A, 2x1 kA to 6x500 A and 3x1 kA for HTS leads in order to accommodate the MARS-D magnet's operation at different frequencies (28 GHz to 45 GHz) and magnetic fields. The higher currents of the leads result in higher heat loads at both 45-50 K and 4.2 K.

The MARS-D cryostat will be built with a hexagonal warm bore to match the shape of the closed-loop coil, maximizing the utilization of the generated radial fields [3]. Correspondingly, the inner bore tubes of the thermal shield and the liquid helium vessel will also be hexagonally shaped. The significant challenge in the cryostat design is the strict space limitation between the magnet's central field and the plasma beam center. The gap between the inner wall of the closed-loop coil and the outer wall of the hexagonal plasma chamber is only 18 mm, as shown in Fig. 2. The available gaps among the hexagonal bore tubes of the LHe vessel, the thermal shield, and the warm vacuum chamber are 2.4 mm and 2.5 mm, respectively.

As shown in Fig. 3, the thermal shield consists of a first-stage cooling plate, an upper neck shield, an outer cylindrical shield assembly, an inner hexagonal shield, flexible copper strips, and their supports. The thermal shield is conduction-cooled by the cryocoolers. The first-stage cooling plate is thermally connected to the cold head of AL330 using flexible OFHC copper links with an appropriate cross-sectional area and is directly connected to copper sleeves brazed onto the drop-in sleeves of the PT450. Indium foils are used at each thermal interface to enhance the effective contact area. The neck shield is either welded or brazed to the first-stage cooling plate. Flexible copper links are used to connect the neck shield and the cylindrical shield assembly to reduce thermal stress during cool down. The cylindrical shield assembly and the hexagonal shield are either welded or brazed together. The upper first-stage cooling plate and neck shield are supported by eight 304SS tubes with a 1/4” outer diameter, 0.035” wall thickness, and 180 mm length. The lower cylindrical shield assembly and hexagonal shield are supported by eight suspension bands made of oriented, enforced fiberglass. Each suspension band is 150 mm long and has a cross-section of 6 mm x 3 mm. Except for the hexagonal shield, the other shields are wrapped with at least thirty layers of multi-layer insulation (MLI) to reduce radiation heat from the outer vacuum chamber (OVC).

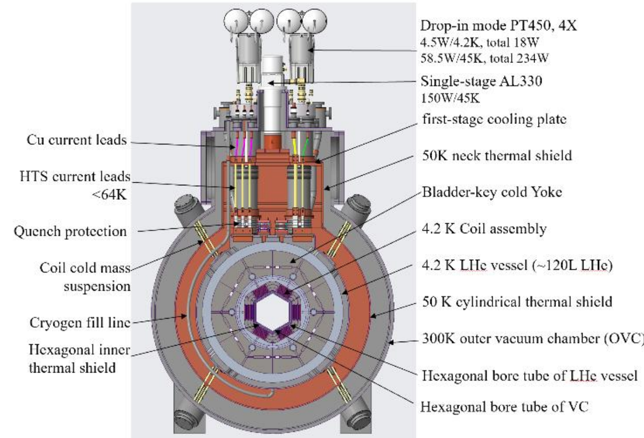

Fig. 2. Cross-sectional view of the MARS-D cryostat.

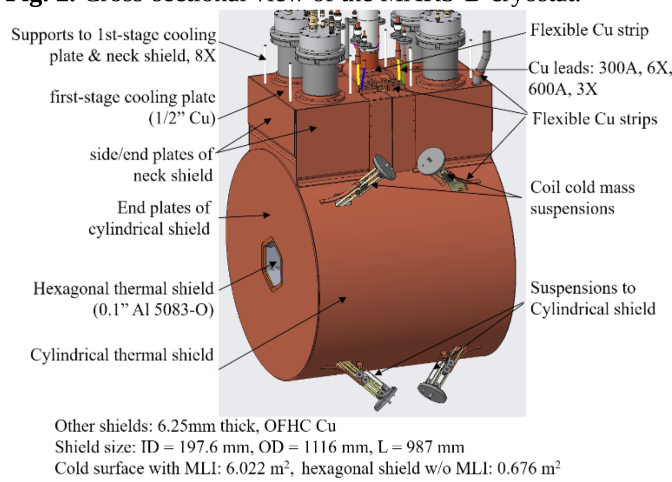

Fig. 3. 3D model design of thermal shield.

Due to the extremely tight space among the hexagonal bore tubes of the LHe vessel, thermal shield, and warm vacuum chamber, it is impossible to apply MLI to help reduce heat loads. Therefore, the material, structure, and thickness of these components must be carefully designed to minimize deformation caused by their weight, thermal stress during cooldown, or the Lorentz force generated by eddy currents induced during magnet excitation, discharge, or in the event of a quench. Thermal-structural simulations and analyses are necessary to ensure sufficient strength of cryostat components and avoid thermal shorts or mechanical contact. This paper focus on the preliminary analyses of the thermal shield.

III. EFFECT OF EDDY CURRENT ON THERMAL SHIELD

During a superconducting magnet quench, the fast-decaying magnetic field induces eddy currents in conductive parts of the cryostat, such as the thermal shield. The generated Lorentz forces can cause significant mechanical stress and deformation. Understanding these forces is crucial for ensuring the structural integrity and safe operation of superconducting magnets. As shown in Fig. 1 and Fig. 2, the magnetic field is shielded by a cold iron yoke located outside the coil assembly, resulting in eddy currents being generated only in inner hexagonally-shaped components, including the bore tubes of the LHe vessel, thermal shield, and warm VC. Due to the high electrical resistivity and strength of stainless steel (316L and 304SS), the forces generated by eddy currents in the bore tubes of the LHe vessel and warm VC are negligible. In this section, the net forces, associated stress distribution, and deformation induced by eddy currents during a quench are analyzed, considering different metallic materials for the shield.

To analyze the eddy currents in the hexagonal shield, the quench behavior of the MARS-D magnet is simulated using OPERA-QUENCH [7], and then the eddy currents are estimated using OPERA-ELEKTRA. The stress and deformation in the hexagonal shield are simulated using ANSYS. The shield is considered symmetric and modeled with a half 3D model to reduce the number of nodes in the finite element analysis (FEA), as shown in Fig. 4. A uniform thickness of 2.5 mm is used for the hexagonal shield.

During a MARS-D magnet quench, the hot spot is assumed to be located at the pole region of the sextupole coil, and the quench propagation is quite fast in it. The coil mandrel acts as a quench back to trigger the quench in the solenoids. The coil current decays rapidly with a time constant of about 3 s.

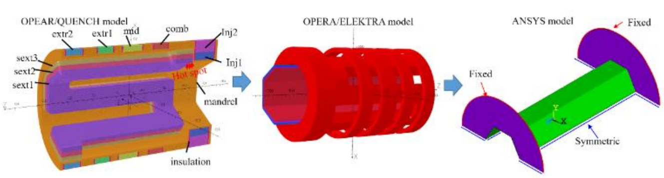

Fig. 4. Simulation models, coil assembly: inner diameter 220 mm, outer diameter 401.5 mm, length 655 mm.

The Azimuthal eddy currents generated in thermal shield,

$$\nabla \times \rho \vec{J} = -\frac{d\vec{B}}{dt} \tag{1}$$

The Lorentz force in the thermal shield,

$$\vec{f} = \vec{J} \times \vec{B} \tag{2}$$

Fig. 5 shows the maximum dynamic force generated in the hexagonal shield made from different materials without electrical cuts: OFHC Cu (RRR=50), Al 1100, Al 6061, Al 5083 during quench. The radial force is the dominant force. The maximum net radial force for OFHC Cu is approximately 105 kN at 0.5-0.8 s, and the maximum net radial force for Al5083 is approximately 2.9 kN at 0.4-0.6 s. However, the maximum net axial force for OFHC Cu is approximately 30 kN at 0.5 s, and the maximum net axial force for Al 5083 is approximately 0.8 kN at 0.4-0.7 s.

Fig. 6 presents the peak stress and maximum deformation on the Al5083 shield during quench, about 28 MPa and 0.5 mm at 0.9 s. Table II summarizes the properties of the shield materials and the comparison results without cuts.

Typically, the use of shield cuts or specific materials can be implemented to mitigate the effects of Lorentz forces and prevent damage. Considering the tight gap constraints (2.4-2.5 mm) among inner hexagonal bore tubes and making the shield a simple structure, Al5083 is preliminarily selected as the material for the hexagonal shield, without electrical cuts. There is no significant stress induced by eddy currents on it during quench, and its relatively small deformation may not cause a thermal short.

IV. Heat Loads And Thermal Analysis

According to the above analysis, Al5083 is preliminarily selected as the material for the hexagonal shield. However, its thermal conductivity is quite low compared to OFHC copper and high-purity aluminum. Due to space constraints, there will be no multi-layer insulation (MLI) wrapped around the inner hexagonal tubes of the LHe vessel and thermal shield. The temperature on the hexagonal shield has a significant impact on the heat loads to 4.2 K, which is studied using FEA thermal simulation in this section.

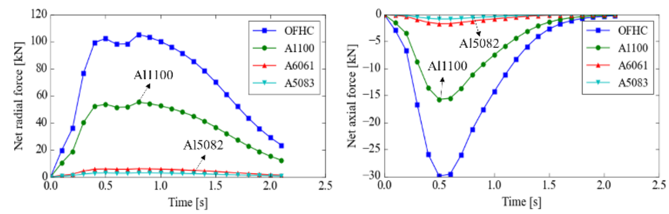

Fig. 5 Dynamic force generated in hexagonal shield made from different materials.

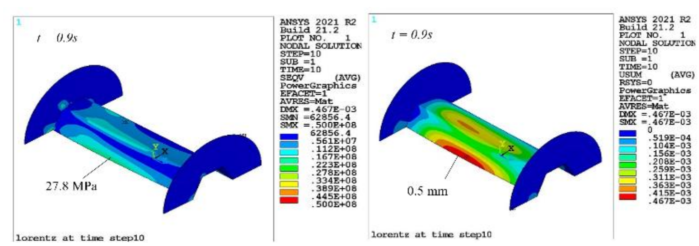

Fig. 6 Peak stress and maximum deformation on Al5083 shield during quench.

Table II Materials' properties and simulation results

Item (@50K)	OFHC Cu	Al 1100	Al 6061	Al 5083
Electrical resistivity (Ω·m)	8.4E-10	1.6E-09	1.48E-08	3.03E-08
Thermal conductivity (W/m/K)	1470	520	52	35
Young's modulus (GPa)	137	77	77.7	80.9
Yield strength (MPa)	90	50	338	179
Ultimate strength (MPa)	310	240	402	557
Net radial force (kN)	105.3	55.3	6	2.9
Net axial force (kN)	-30	-15.7	-1.7	-0.8
Maximum stress (MPa)	2310	1040	112	55
Maximum deformation (mm)	20.8	9.6	1.1	0.5

A. Estimates of Heat Loads

The heat load to the MARS-D shield is estimated including (1) radiation heat inleak from the OVC to the shields with and without MLI; (2) conduction heat inleaks from the intermediate thermal intercepts for 4.2 K suspensions, cryogen fill tube, and vent tube between the OVC and LHe vessel; (3) conduction heat flow through supports and suspensions of the shields, and through instrumentation leads; and (4) heat loads generated by copper leads. Fig. 7 presents the estimated heat loads to the 45 K stage of the cryocoolers. The dominant loads are from the nine current leads and heat radiation to the thermal shield. The total heat load is estimated to be 272 W without any contingency. The total cooling capacity provided by the coolers is 384 W at 45 K, which can cover the loads.

B. Thermal Analysis

The following assumptions have been made for the thermal simulation: (1) the 45 K stage of the cryocoolers and the first-stage cooling plate are in perfect contact; (2) a 10% cooling capacity loss due to drop-in-mode sleeves of the PT450 cryocoolers; (3) a 50% effective contact area for all welded joints; (4) the estimated heat loads are distributed on the shield as shown in Fig. 7; and (5) except for the hexagonal shield, the other shields are made of OFHC Cu (RRR=100) with 6.25 mm thickness. Temperature-dependent properties of the thermal conductivity for each material are taken from references [8]. The maximum temperature on the first-stage cooling plate is expected no higher than 60 K, which is limited by the working temperature of HTS leads <64 K.

For concentric hexagonal tubes with tiny gaps, assuming emissivity $\varepsilon 1=\varepsilon 2=0.1$ for polished surface, view-factor=1, surface $A1=A2=A$, $\sigma=5.67\times10^{-8}$ W/m²·K⁴, high and cold temperature T_1 and T_2, the radiation heat flux about 25 W/m² estimated by the following equation was applied to the hexagonal shield,

$$q = \sigma A(T_1^4 \text{-} T_2^4)/(\frac{1}{\varepsilon 1}+\frac{1}{\varepsilon 2}-1) \tag{3}$$

Fig. 8 shows the steady-state temperature distribution over the whole shield. The maximum temperature of 72.3 K is in the middle of the hexagonal shield. The temperature at both ends of the hexagonal shield is approximately 46.5 K, but it increases rapidly toward the center. The maximum temperature in the area of the warm-end of HTS leads on the first-stage cooling plate is approximately 47 K (< 60 K). High temperature on the hexagonal shield will result in high heat loads to 4.2 K. The radiation heat flux from the 80 K hexagonal shield to the 4.2 K LHe vessel is about 0.122 W/m², assuming ε=0.1.

Lower surface emissivity ε will decrease the radiation heat flux. As compared in Table III, at the same ε, the heat flux from 80 K to 4.2 K is about 6.5 times than that from 50 K to 4.2 K. Polished, clean surfaces yield lower emissivity, but ε increases rapidly with oxidation, contamination, impurities, dirt, roughness, and so on. Great care needs to be taken in practical operation to retain low surface emissivity.

Fig. 9 presents the simulation results under various radiation heat fluxes. With decreasing radiation heat flux (ε), the maximum temperature on the hexagonal shield decreases. Radiation heat flux only has a significant impact on the temperature along the hexagonal shield. The temperature at its both ends changes slightly, and the temperature in the area of the warm-end of HTS leads on the first-stage cooling plate remains almost unchanged.

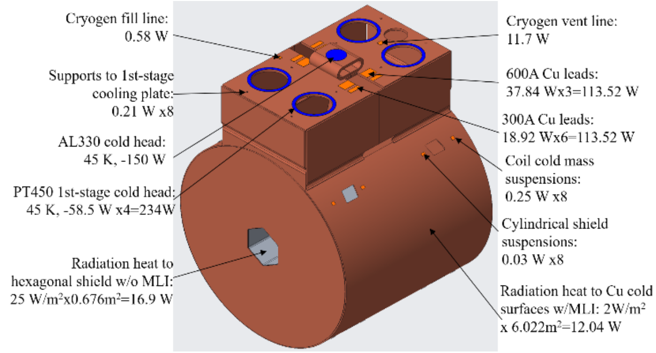

Fig. 7 Heat loads to the MARS-D thermal shield.

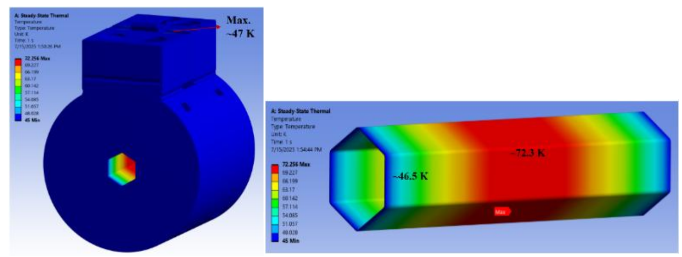

Fig. 8 Temperature distribution over the shield.

Table III. Radiation Heat flux vs surface emissivity w/o MLI

Emissivity (ε)	50-4.2K q (W/m²)	300-50K q (W/m²)	80-4.2K q (W/m²)	300-80K q (W/m²)
0.05	0.0091	11.77	0.06	11.72
0.1	0.0187	24.15	0.122	24.05
0.18	0.035	45.39	0.23	45.19

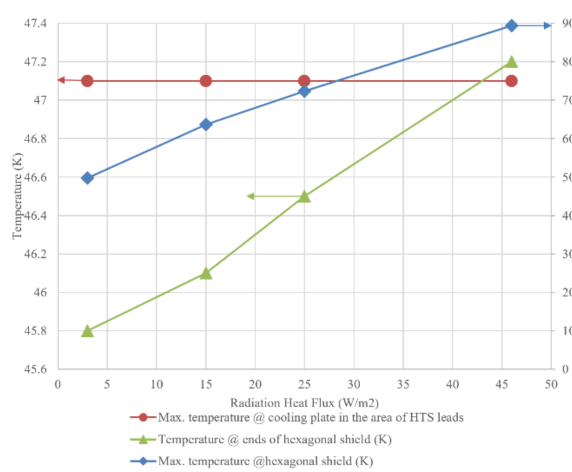

Fig. 9 Temperatures on the shield at different heat flux.

V. Conclusion

To reduce stress and deformation generated by eddy currents during a quench, the MARS-D thermal shield is designed with two materials: a 2.5 mm thick Al5083 hexagonal shield and 6.25 mm thick OFHC copper shields. To reduce radiation heat flux to 4.2 K and the temperature on the hexagonal shield, highly polished and clean surfaces attached with low emissivity Al foil will be applied. Further FEA simulations will study overall stresses and deformation caused by weight, vacuum pumping, cooldown, and Lorentz forces during magnet quench.

REFERENCES

[1] D. Z. Xie, J. Y. Benitez, A. Hodgkinson, T. Loew, C. M. Lyneis, L. Phair, P. Pipersky, B. Reynolds, and D. S. Todd, “Design of a New Superconducting Magnet System for High Strength Minimum-B Fields for ECRIS,” *IEEE Trans. Appl. Supercond.*, vol. 26, no. 4, pp. 1–5, 2016, doi:10.1109/TASC.2015.2511928.

[2] D. Z. Xie, J. Y. Benitez, A. Hodgkinson, T. Loew, C. M. Lyneis, L. Phair, P. Pipersky, B. Reynolds, and D. S. Todd, “Development status of a next generation ECRIS: MARS-D at LBNL,” *Rev. Sci. Instrum.*, vol. 87, p. 02A702, 2016, doi: 10.1063/1.4931713.

[3] D. Z. Xie, J. Y. Benitez, M. Kireeff Covo, A. Hodgkinson, M. Juchno, L. Phair, D. Todd, and L. Wang, “STATUS OF THE 45 GHz MARS-D ECRIS,” in *ECRIS-2020*, Virtual WS, Lansing, MI, September 2020, doi: 10.18429/JACoW-ECRIS2020-MOXZO01.

[4] L. Wang, D. Xie, J. Y. Benitez, L. Xu, L. W. Phair, M. Juchno, P. Ferracin, "Preliminary Design of a MARS-D Superconducting Magnet Cryostat," MT28-3PoA01-01, *the MT-28 conference*, Aix-en-Provence, France, September 10-15, 2023.

[5] M. Juchno, J. Y. Benitez, J. Doyle, A. Hodgkinson, T. Leow, L. W. Phair, D. S. Todd, L. Wang, and D. Z. Xie, “Shell-Based Support Structure for the 45 GHz ECR Ion Source MARS-D,” *IEEE Trans. Appl. Supercond.*, vol. 32, no. 6, pp. 1–5, 2022, doi: 10.1109/TASC.2022.3158375.

[6] L. Xu, J. Benitez, J. C. Duran, P. Ferracin, M. Juchno, L. Phair, D. Todd, L. Wang, D. Xie, and Y. Yang, “Fabrication of an NbTi Superconducting Closed-loop Coil for the Next-generation 45 GHz ECR Ion Source MARS-D,” *IEEE Trans. Appl. Supercond.*, vol. 35, no. 5, 2025, doi:10.1109/TASC.2025.3542743.

[7] Y. Yang, “Eddy current induced Magnetic force in thermal shield during the quench,” *internal progress report*, LBL, 2024-2025.

[8] “Index of Material Properties”, NIST [Online]. Available: https://trc.nist.gov/cryogenics/materials/materialproperties.htm.